

An H-Shaped Differential Fed Patch Antenna for a GaN Base Station Transmitter

Rida Gadhafi*, Dan Cracan, Ademola A. Mustapha, and Mihai Sanduleanu

Abstract—In this paper, a differentially fed, structurally simple, patch antenna, operating at 5.2 GHz is presented. The proposed antenna is particularly designed for a base station, Gallium Nitride (GaN) transmitter. The antenna is composed of an H-shaped patch, backed by a ground plane, with two differential feeds placed at the longitudinal edges. The size of the antenna is $0.55\lambda_0 \times 0.49\lambda_0 \times 0.27\lambda_0$ (where λ_0 is the free space wavelength at the center frequency). A prototype of the stand-alone antenna is designed, fabricated, and measured. The antenna offers a voltage standing wave ratio (VSWR) bandwidth of 4% and a differential impedance of $100\ \Omega$, which matches most of the differential integrated circuits. The measured gain and directivity of the proposed differential antenna are 5.3 dBi and 7 dB, respectively. From simulation it is observed that the proposed antenna possesses a front to back ratio of 15.69 dB and a 3 dB beamwidth of 84° . The measured peak efficiencies of the antenna in the lower and higher bands are 84% and 59%, respectively. Details of the design and lumped model, along with the experimental and simulated results, are presented and discussed. The effect of scaling different design parameters for operation at different frequency bands is considered as well.

1. INTRODUCTION

Most of the Radio Frequency (RF) circuits in wireless communication are in differential form as this configuration improves the rejection of strong common mode fields present at the differential input ports or differential output ports [1, 2]. To fulfill the ever increasing demand for signal integrity in modern wireless communication systems, diverse differential antennas have been studied and evaluated in the literature. Dipole and loop antennas are the most common structures used in differential configurations [3–5]. However, the gain for such antennas is limited, and hence the overall efficiency of the system is reduced.

Microstrip antennas, owing to their small size, high gain, low profile, low cost, and ease of fabrication, represent good candidates for wireless communication, where differential input/output is needed [6–7]. Research efforts have been focused on developing microstrip patch antennas with improved gain and efficiency [7–12]. However, most of them follow stacked or low temperature co-fired ceramics (LTCC) layers rendering the whole system complicated and expensive [8–15]. Furthermore, only a few of them employ double layered designs [15–18]. In the area of consumer applications, where we need performance at low cost, a structurally simple antenna with improved gain is in high demand.

Additionally, antennas and bandpass filters are two vital components present in the RF front-ends. To achieve a maximum power transfer, it is important to maintain the impedance matching between these two components. Use of additional matching networks will increase form factor and makes the system complicated and expensive. Hence, antennas with $100\ \Omega$ differential impedance have a significant role in wireless communication systems, as they can be matched to many of the standard integrated

Received 6 February 2019, Accepted 2 April 2019, Scheduled 19 April 2019

* Corresponding author: Rida Gadhafi (rida.gadhafi@ku.ac.ae).

The authors are with the Khalifa University of Science and Technology, Abu Dhabi 127788, United Arab Emirates.

components. Even though several investigations on double layer differential antennas can be seen in the literature, matching the differential impedance to $100\ \Omega$ is seldom found.

The proof of concept of the antenna is already explained in [17]. This paper provides the full analysis: analytical, simulated, and experimental characterizations of the proposed differential antenna. It presents an accurate lumped model of the antenna together with its discontinuity impact and compares the circuit and electromagnetic simulation models along with the experimental characterization. The power transfer capability of the proposed antenna for different distances is also discussed. The antenna exhibits a differential impedance of $100\ \Omega$ and 2 : 1 VSWR bandwidth of 4%. For characterization and measurement purposes, RF integrated circuits have $50\ \Omega$ terminations to either ground or voltage supply, rendering a $100\ \Omega$ termination impedance, in differential mode. The size of the antenna is $0.55\lambda_0 \times 0.49\lambda_0 \times 0.27\lambda_0$ (where λ_0 is the free space wavelength at the center frequency) and could be scaled accordingly for a specific application. The proposed antenna has a measured gain of 5.3 dBi and directivity of 7 dB at the center frequency. The simulated front-to-back ratio across the operating band is 15.69 dB. The measured peak efficiencies of the antenna in the lower and higher bands are 84% and 59%, respectively.

The rest of the paper is organized as follows. Section 2 presents the antenna architecture and design together with the derivation of a lumped model. Section 3 presents the simulated versus measured results and the discussion on the discrepancies between the two. Section 4 presents a benchmark and a comparison based on published data from literature. Section 5 concludes the paper.

2. ANTENNA DESIGN, SCALING AND LUMPED MODEL

The design, model, and simulations of the proposed antenna are discussed in this section. Electromagnetic simulations are performed using Ansys HFSS whereas Cadence Virtuoso is used for validating the lumped model.

2.1. Antenna Design

Figure 1 shows the application diagram of the GaN transmitter bond-wired to a PCB. Multiple bond wires (4 in this case) are used to reduce the inductance of the bond wire ($\sim 1\ \text{nH}$). The output terminal of the GaN chip with a differential output impedance of $18\ \Omega$ is connected to a differential bandpass filter, through a customized matching circuit (Klopfenstein taper) and thereafter to a differential antenna. Each output A of the GaN chip is connected to the supply V_{DD} with an inductor L being a part of a resonant circuit. Both filter and antenna are designed for $50\ \Omega$ in single-ended mode. Each GaN power amplifier (PA) generates 10 dBm output power, and multiple PA + filter + antenna units are organized in an array for power combining and beam steering. The geometry of the proposed stand-alone antenna is

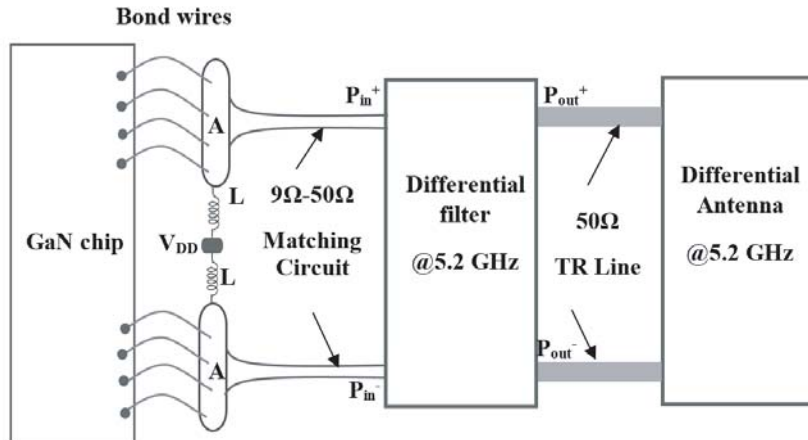


Figure 1. Application diagram of the proposed GaN base station transmitter unit (10 dBm power/unit).

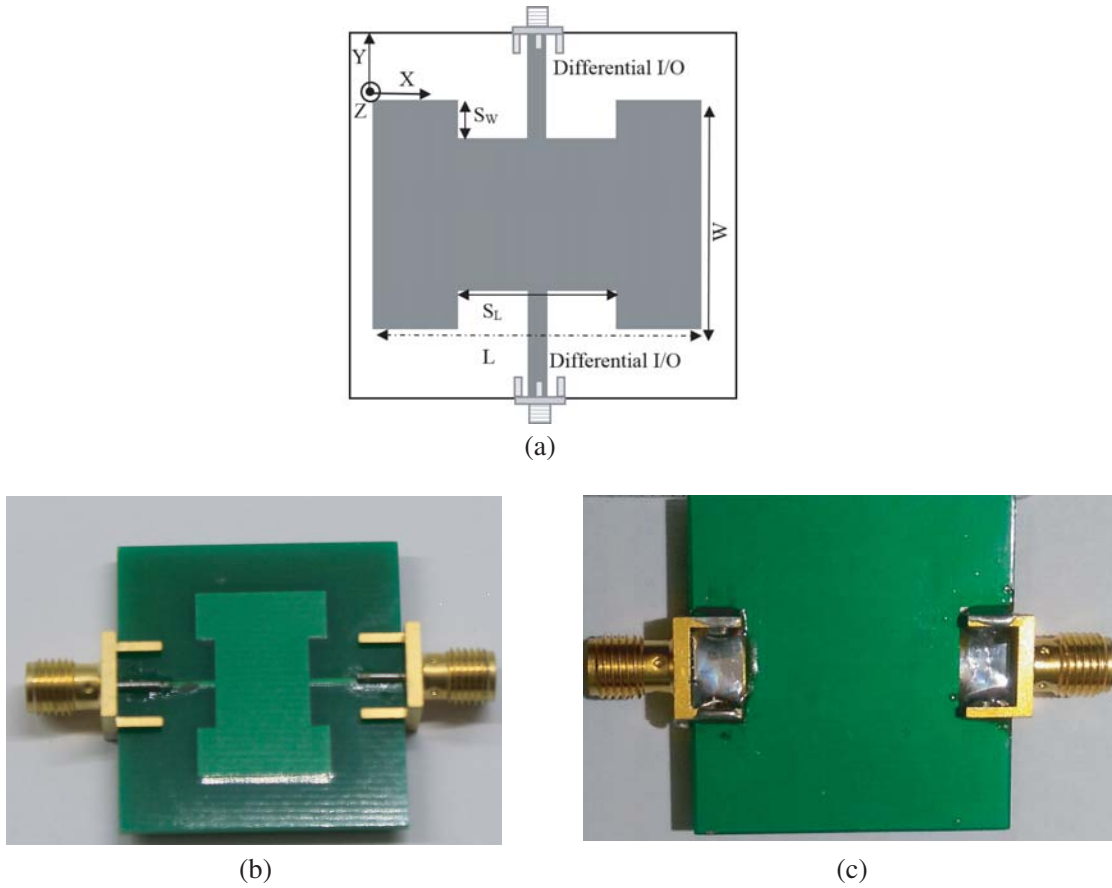


Figure 2. Geometry of the stand-alone antenna; (a) geometry of the antenna. Fabricated antenna (b) top view, (c) bottom view ($S_W = 2\text{ mm}$, $W = 14\text{ mm}$, $L = 20.7\text{ mm}$, $S_L = 10\text{ mm}$; $\epsilon_r = 4.4$, $\tan \delta = 0.015$, and $h = 1.6\text{ mm}$).

shown in Fig. 2(a), with the top and bottom views of the fabricated antenna in Fig. 2(b) and Fig. 2(c), respectively. The antenna is derived from a conventional inset-fed rectangular patch antenna. Further, it is transformed to a differential design by integrating differential feeds at the longitudinal edges. The inset-length S_L and inset-distance S_W are optimized for frequency tuning and better impedance matching. We find that the differential impedance of the antenna can be controlled by optimizing the dimensions of this inset slot. The dimensions of the proposed antenna are optimized for the frequency of interest. The frequency of operation (f_C) of the antenna is found to be the same as the standard half wave patch and is given as follows:

$$f_C = \frac{c}{2W\sqrt{\epsilon_r}}, \tag{1}$$

where c is the speed of light, W the width of the H-shaped patch antenna, and ϵ_r the permittivity of the substrate used [19]. It is noticed that patch length L mainly influences the impedance matching of the antenna, with a small shift in frequency. In contrast, a change in the width of antenna W creates a large frequency shift (e.g., for a 1 mm change in length L , the antenna experiences a 30 MHz frequency shift, while the same change in W produces a frequency shift of 300 MHz when $f < f_C$ and 60 MHz when $f > f_C$). The intrinsic antenna has a size of 2.07 cm \times 1.4 cm. The differential impedance of the antenna needs to be matched with the input impedance of the device under test. For a stand-alone antenna, a microstrip feed line is used. This can be connected to the two inputs of the differential device under test, such as a Low Noise Amplifier (LNA) or a Power Amplifier (PA); a differential filter in this context. The width of the feed line is optimized to obtain the differential impedance of 100 Ω . This is a standard impedance value for most of the differential circuits connected to the measurement equipment

or antenna. The differential impedance (Z_{diff}) of the microstrip patch antenna can be calculated by considering it as a two-port network and using the following formula [20, 21]:

$$Z_{\text{diff}} = 2Z_0 \frac{1 - s_{11}^2 + s_{21}^2 - 2s_{21}}{(1 - s_{11})^2 - s_{21}^2} \quad (2)$$

This differential impedance is a function of the substrate parameters and dimensions of the patch [8].

2.2. Parametric Study and Optimization of the Differential Antenna

The differential antenna is designed at 5.2 GHz. The H-shaped patch and ground are on a low cost FR-4 substrate with a dielectric constant of 4.4, tangent loss of 0.025, and thickness of 1.6 mm. The dimensions of the antenna can be optimized to match the frequency requirements, and the differential impedance of the feed line can be optimized to match the standard impedance value of the device under test. This section presents the parametric simulations performed in order to optimize the design parameters. The influence of inset-length (S_L) and inset-distance (S_W) on antenna characteristics is studied. Firstly, the variation of the differential return loss (S_{11dd} -parameter) of the proposed antenna with different inset-lengths is studied, and we find that frequency tuning is achieved with different inset-lengths. Approximately 1 GHz frequency tuning is achieved with a change in inset-length from 1 mm to 18 mm [17]. This is the maximum allowed change as per the dimension of the proposed antenna. The optimum inset-length can be chosen in accordance to the frequency of interest. Additionally, the real and imaginary parts of the differential impedance are inversely proportional to the inset-length. Parametric simulation shows that with an optimum value of slot length, the real part of the differential impedance is 100Ω , and the imaginary part of the differential impedance is 0Ω at frequency of resonance. This is ideal for differential circuits that have an input/output impedance of 50Ω with respect to ground or power supply at each arm [21], allowing maximum power transfer with the input devices like LNAs or PAs. From simulations we find that the inset-distance determines the impedance matching of the antenna. Thus, the optimum values for inset-length and inset-distance are chosen as 10 mm and 2 mm, respectively. Fig. 3 shows the surface current distribution of the antenna at 5.2 GHz. The current is maximum along the width (W) of the antenna. It is clear that the antenna radiates at its edges, and the frequency of operation is governed by the width W , as already given by Equation (1).

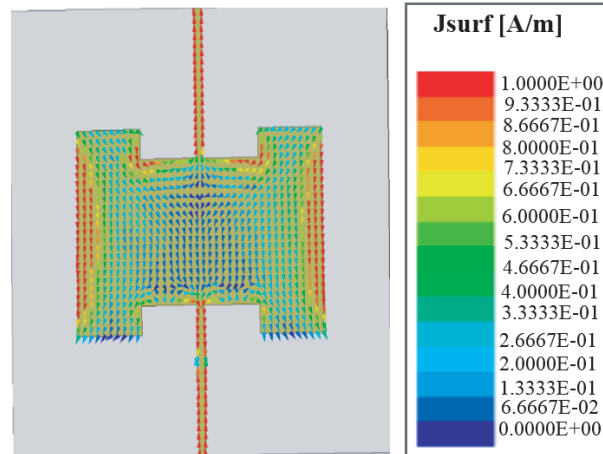


Figure 3. Simulated surface current distribution of the proposed antenna in differential mode at 5.2 GHz.

From the simulation studies, using HFSS, the optimum design parameters of the antenna, as a function of guided wavelength, λ_g , are $S_L = 0.3\lambda_g$, $W = 0.42\lambda_g$, and $L = 0.62\lambda_g$. The design parameters are validated for different frequencies.

2.3. Equivalent Circuit Modeling of the Differential Antenna

The equivalent circuit model of the proposed antenna has been studied and evaluated. The proposed differentially fed antenna is modeled as three sections, as shown in Fig. 4(a): (i) a microstrip feed line (Fig. 4(b)), (ii) a grounded coplanar waveguide (CPW) (Fig. 4(c)), and (iii) a microstrip transmission line (Fig. 4(d)). In order to obtain an accurate model, the discontinuity impact has also been studied as explained in [22]. The validation of this model is performed in Cadence Virtuoso using Spectre RF. Fig. 4 shows the top views of these three different sections.

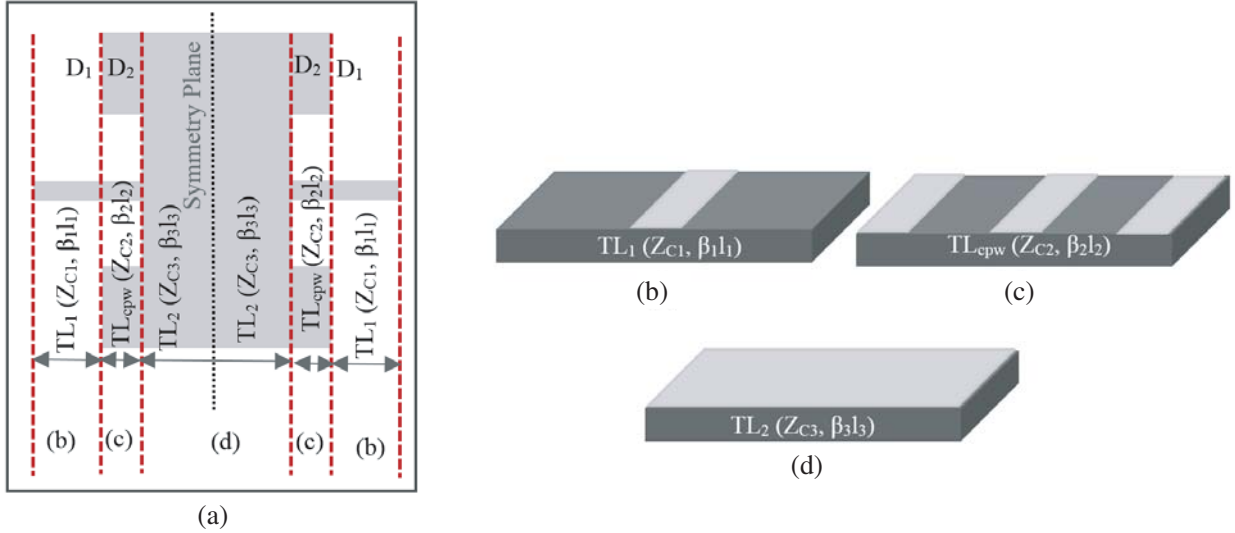


Figure 4. Three different sections of the proposed differential fed antenna used for equivalent circuit model study. (a) Modeled top patch, (b) microstrip feed line, (b) conductor backed CPW and (c) microstrip transmission line. Only top layer is demonstrated here.

The microstrip feed line TL_1 has a characteristic impedance Z_{C1} and propagation constant β_1 . Similarly, the grounded CPW line has a characteristic impedance Z_{C2} and propagation constant β_2 . The third part is defined as a microstrip transmission line TL_2 with characteristic impedance Z_{C3} and propagation constant β_3 . D_1 and D_2 represent the two discontinuities. To include the effect of these two discontinuities, we follow the approach explained in [22]. For each section of the antenna, a chain matrix is used, where $[C_1]$ is the chain matrix for the transmission line TL_1 , $[D_1]$ the chain matrix for the discontinuity D_1 , $[C_2]$ the chain matrix for the grounded CPW, $[D_2]$ the chain matrix for the discontinuity D_2 , and $[C_3]$ the chain matrix for the transmission line TL_2 . Thus the equation of the chain matrix of the proposed differential fed antenna is:

$$[C_T] = [C_1][D_1][C_2][D_2][C_3^1][C_3^2][D_2][C_2][D_1][C_1], \quad (3)$$

where $[C_3^1]$ and $[C_3^2]$ are the chain matrices of the two halves of the transmission line TL_2 . As the antenna is symmetrical, $[C_T]$ can be divided into two parts and $[C_T] = [C_{TL}][C_{TR}]$. The matrices for the left and right planes are:

$$[C_{TL}] = [C_1][D_1][C_2][D_2][C_3^1], \quad (4)$$

$$[C_{TR}] = [C_3^2][D_2][C_2][D_1][C_1], \quad (5)$$

where $[C_{TL}]$ and $[C_{TR}]$ are the chain matrices of the left and right symmetrical planes, respectively, in single ended configuration. Each chain matrix can be expressed in terms of S -parameters. For each antenna part we perform S -parameter simulations. Hence, in order to solve Equation (4), two frequency points, f_a and f_b , around the resonance frequency f_c have been considered. Thus Equation (4) can be rewritten in terms of these two frequency points as:

$$\begin{aligned} [C_{TL}]_{f_a} &= [C_1]_{f_a}[D_1][C_2]_{f_a}[D_2][C_3^1]_{f_a} \\ [C_{TL}]_{f_b} &= [C_1]_{f_b}[D_1][C_2]_{f_b}[D_2][C_3^1]_{f_b}, \end{aligned} \quad (6)$$

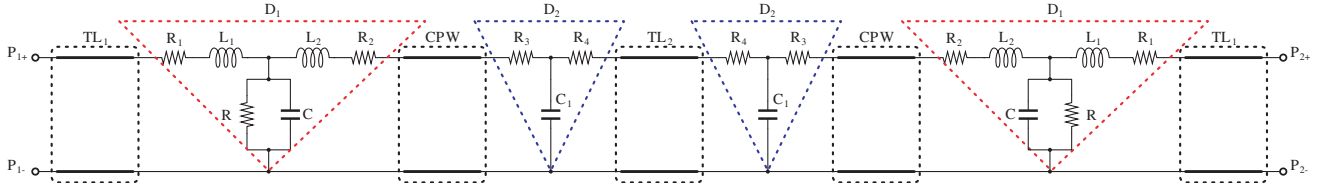


Figure 5. Equivalent circuit of the proposed differential fed antenna with discontinuities D_1 and D_2 .

The values of the discontinuity matrices $[D_1]$ and $[D_2]$ can be solved from Equation (6) using the approach explained in [22]. The equivalent circuit of the proposed differentially fed patch antenna including the symmetrical discontinuities D_1 and D_2 is shown in Fig. 5. This is obtained by composing three different sections, as explained in Fig. 3, in series, as in the layout of the differential fed patch antenna. As shown in Fig. 5, each discontinuity is associated with an impedance T-network, and by solving D_1 and D_2 , the impedance values can be extracted. The values of the lumped components used are listed in Table 1. As already stated, as the antenna is symmetrical, the circuit components are repeated. Fig. 6 shows the comparison of the differential S_{11} parameters in dB, for circuit simulation and electromagnetic simulation.

Table 1. Lumped element values used for the equivalent circuit.

R (Ω)	L (nH)	C (fF)
$R = 750$	$L_1 = 4.25$	$C = 680$
$R_1 = 1.8$	$L_2 = 1.1$	$C_1 = 100$
$R_2 = 3.9$		
$R_3 = 0.9$		
$R_4 = 0.82$		

3. MEASUREMENT RESULTS AND DISCUSSION

As reported in [19], the antenna has been characterized using an Agilent Network Analyzer (PNA-X N5242A) and a commercially available balun from Marki Microwave [23]. The balun can operate between 1.2 GHz and 6 GHz, and provides $50\ \Omega$ to $100\ \Omega$ differential transformation. The balun has a single input and two outputs with 180° phase shift with respect to each other.

As shown in Fig. 7, the input of the balun is connected to one port of the PNA, and the two output ports of the balun are connected to the two differential arms of the antenna. The corresponding reflection coefficient has been measured. Fig. 8 shows the simulated and experimental return loss characteristics of the antenna. It is found that measurement results show a performance degradation due to the external balun used. The manufacturer datasheet shows that the balun introduces -3.6 dB of frequency dependent losses throughout its frequency of operation band (1.2 GHz–6 GHz) [23]. The antenna shows a 2 : 1 VSWR bandwidth of 200 MHz in the 5.2 GHz band from 5.1 GHz to 5.3 GHz. The bandwidth of the antenna can be further enhanced using the technique shown in [24].

Figure 9 shows the simulated 3-D radiation pattern of the antenna. As seen, the antenna produces a unidirectional pattern. The radiation patterns in the orthogonal planes are measured inside an anechoic chamber and are shown in Fig. 10(a) and Fig. 10(b) along with the simulated patterns. The measured results show reasonably good agreement with the simulated ones. However, a slight discrepancy can be observed due to the balun and coaxial cables used for the measurement.

As seen in Fig. 10, the antenna provides a broadside radiation pattern in the y - z plane. The co-polar and cross-polar isolation in the horizontal plane (E -plane or y - z plane) is in the order of -12 dB and around -17 dB in the vertical plane (H -plane or x - z plane). From the simulation results, it can be seen that the antenna possesses a front to back ratio of 15.69 dB across the operating band. The 3 dB

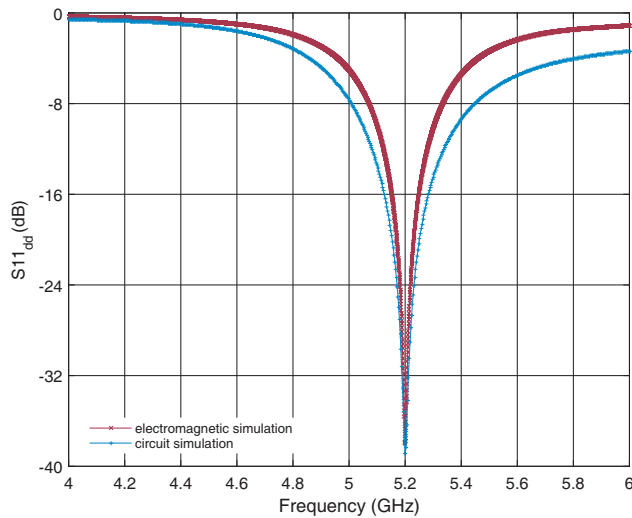


Figure 6. Comparison of the S_{11} parameters between electromagnetic and circuit simulation.

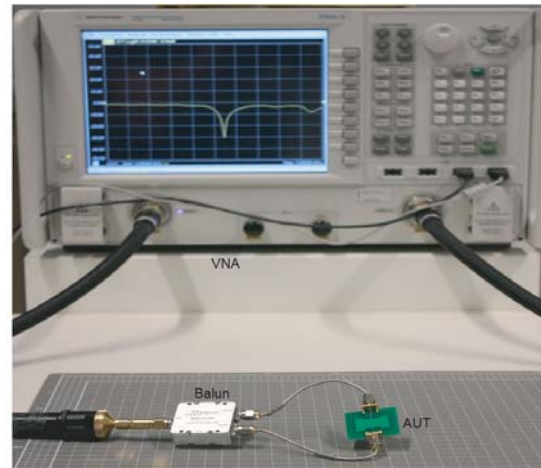


Figure 7. Measurement setup of the antenna together with commercially available balun for characterizing differential S -parameter.

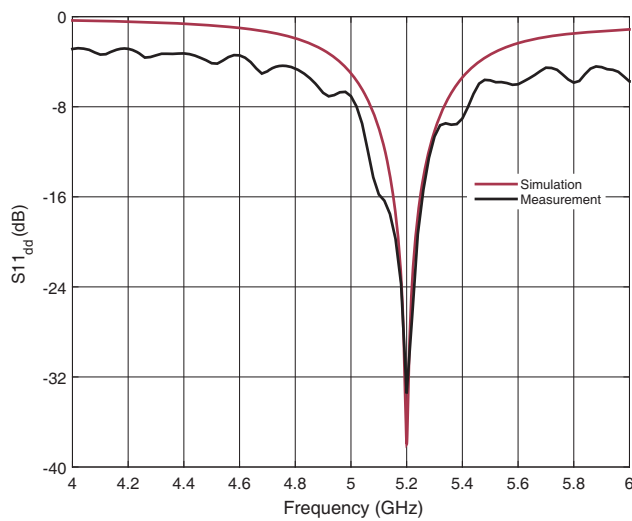


Figure 8. Simulated and measured return loss characteristics of the proposed antenna ($S_W = 2$ mm, $W = 14$ mm, $L = 20.7$ mm, $S_L = 10$ mm; $\epsilon_r = 4.4$, $\tan \delta = 0.015$, and $h = 1.6$ mm).

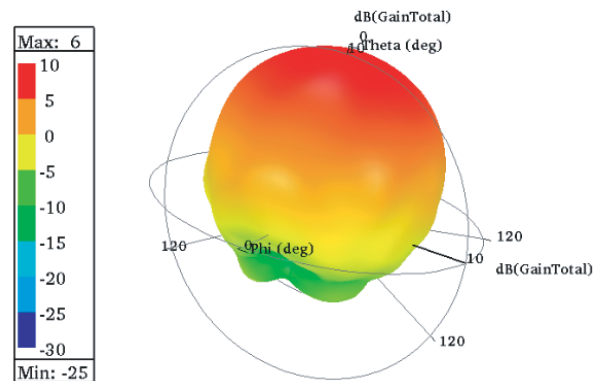


Figure 9. 3-D radiation pattern of the proposed differential antenna.

beamwidth of the antenna along co-polar E -plane and H -plane is 84° .

The gain is measured by the gain comparison method in the boresight direction. Fig. 11 depicts the measured gain in comparison with the simulated gain. It is found that the peak simulated gain of 5.68 dBi is achieved at 5.2 GHz. However, the measured peak gain is slightly shifted to the lower frequency (5.12 GHz) and is found to be 5.3 dBi. Moreover, the measured antenna gain is not uniform in contrast to the simulated gain, where a uniform gain can be observed in the operating bandwidth. The discrepancy is due to the frequency dependent losses of the external balun used, which will be eliminated while connecting the antenna directly to the differential RF circuit. The antenna exhibits a directivity of 7 dB. The measured peak efficiencies of the antenna in the lower and higher bands are

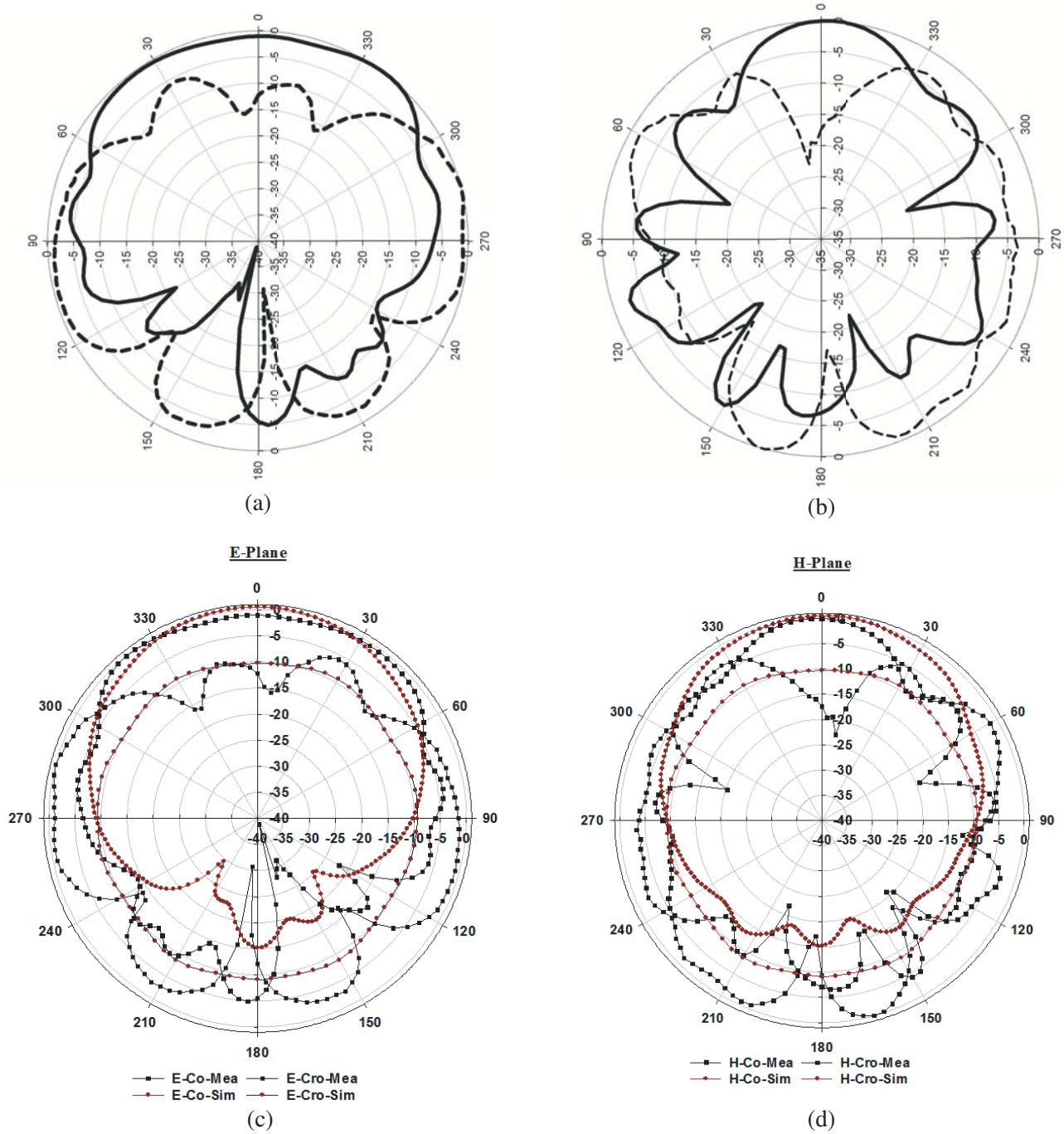


Figure 10. Measured and simulated radiation pattern of the proposed differential antenna at 5.2 GHz. (a) Measured co (solid line) and cross (dashed line) polarization in *E*-plane, (b) measured co (solid line) and cross (dashed line) polarization in *H*-plane, (c) simulated and measured co and cross polarization in *E*-plane, (d) simulated and measured co and cross polarization in *H*-plane.

84% and 59% respectively as shown in Fig. 12.

The power transfer measurement of the proposed antenna has also been conducted as explained in [24]. Two identical antennas separated with a distance d are placed face to face. The antennas are connected to the two ports of the Network Analyzer, and corresponding S_{21} is measured. Two baluns are used to perform this measurement. The power receiving capability of the antenna is tested for different

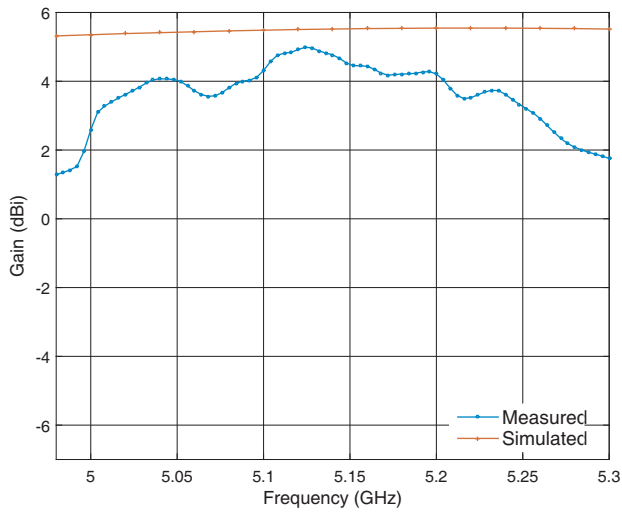


Figure 11. Simulated and measured gain versus frequency of the differential antenna.

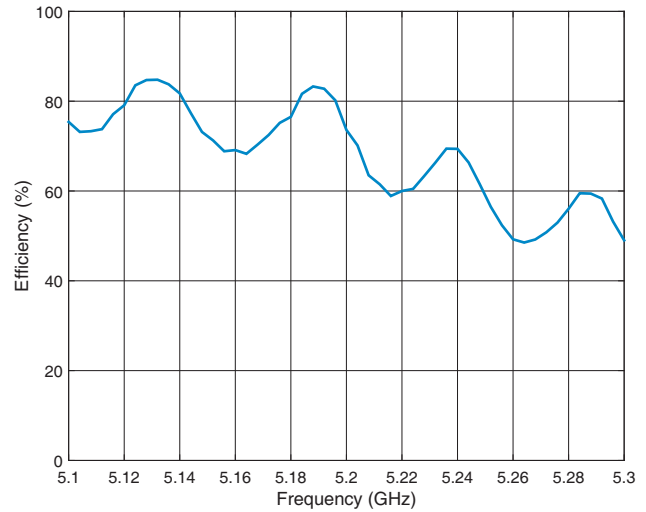


Figure 12. Measured efficiency of the differential antenna.

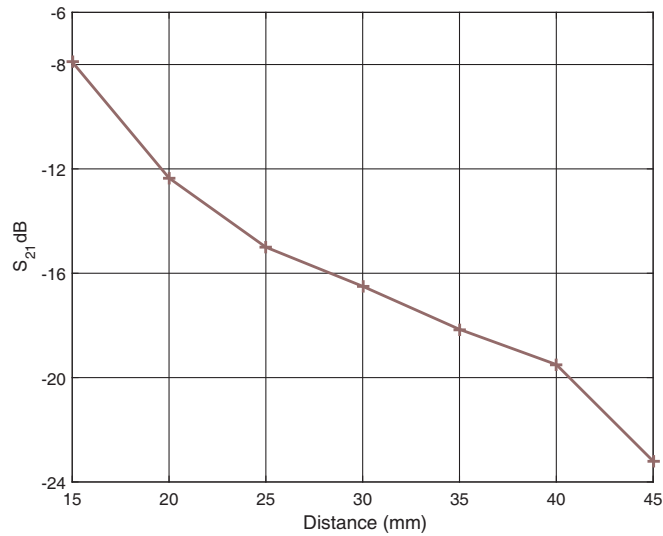


Figure 13. Power transfer capability of the proposed antenna. Received power versus distance between the two antennas.

distances. The magnitude of the power received (S_{21}) including the losses from two baluns is shown in Fig. 13. As seen, the magnitude of power decreases with increasing distance. The measurement is conducted for a range d from 1.5 cm to 4.5 cm.

4. BENCHMARK AND DISCUSSION

Table 2 shows the summary of some previously published differential antennas compared with the proposed one. As can be seen, most of the published works follow a stacked or LTCC type of structure except [12] and [16] where double-layer structures are used. Even though such structures have high performance compared to the two-layer microstrip structures, the stacked configuration will render the whole system complicated and expensive. Moreover, contrary to LTCC structures, FR-4 structures are cheap and easy to implement. As shown in Table 2, among the reported double layer antennas, [11] is

Table 2. Benchmark between the proposed design and reported works.

Ref.	Substrate	Layers	Size (cm ²)	Freq. (GHz)	Gain (dBi)
[8]	FR-4	Stacked	13.7 × 13.7	0.87–1.05	8.5
[9]	LTCC	Stacked	2.4 × 1	4.1–4.5	8
[10]	FR-4	Stacked	2 × 2	2.4, 5.2	1, 5
[11]	PCB	Stacked	NA	3.5	8.3
[12]	FR-4	double layer	7.1 × 7.9	2.8–6.4 (UWB)	2.4 @ 4 GHz
[14]	LTCC	Stacked, 4 × 4 antenna array	1.4 × 1.5	60	18.62
[16]	FR-4	double layer	6 × 5	2.45	2.3
this work	FR-4	double layer	2.07 × 1.4	5.2	5.68

a UWB antenna, and [16] is a bow-tie antenna. Compared to these antennas, microstrip antennas are more robust owing to their full ground plane, which is very significant while connecting the antennas to the RF front ends. Thus, as already stated, the proposed antenna is a structurally simple antenna with moderate gain, high robustness, unidirectional radiation pattern, and small form factor.

5. CONCLUSION

A structurally simple, H-shaped, differential patch antenna operating at 5.2 GHz is fabricated and measured. The proposed antenna is particularly designed for a base station, GaN transmitter. The size of the antenna is $0.55\lambda_0 \times 0.49\lambda_0 \times 0.27\lambda_0$ (where λ_0 is the free space wavelength at the center frequency). Experimental results show that the proposed antenna has a VSWR < 2 for frequencies between 5.1 GHz and 5.3 GHz. It also exhibits a gain of 5.68 dBi and a unidirectional radiation pattern. The simulated front to back ratio is 15.69 dB across the operating band. The measured efficiency of the antenna is 84% in the lower band and 59% in the higher band. The simulated 3 dB beamwidth of the antenna along co-polar E -plane and H -plane is 84° . The antenna has a differential impedance of 100Ω which matches most of the integrated circuits that have 100Ω differential impedance. A lumped model of the antenna has been designed and evaluated. Measurements show that the model fits the electromagnetic design. The power transfer capability of the antenna is also tested. Based on parametric simulations, the antenna could be scaled at different frequencies, and insights on how to perform frequency scaling are included in the paper.

REFERENCES

1. Ding, C. and K. M. Luk, "Compact differential fed dipole antenna with wide bandwidth stable gain and low cross polarization," *Electronic Letters*, Vol. 53, No. 15, 1019–1021, 2017.
2. Xue, Q., X. Zhang, and C. H. Chin, "A novel differential fed patch antenna," *IEEE Antennas Wirel. Propag. Lett.*, Vol. 5, No. 1, 471–474, 2006.
3. Gadhafi, R., D. Cracan, A. A. Mustapha, and M. Sanduleanu, "A tuning fork shaped differential dipole antenna with floating reflectors," *Progress In Electromagnetics Research Letters*, Vol. 80, 47–52, 2018.
4. Kotani, K., A. Sasaki, and T. Ito, "High efficiency differential drive CMOS rectifier for UHF RFIDs," *IEEE J. Solid-State Circuits*, Vol. 44, No. 11, 3011–3018, 2019.
5. Le, T., K. Mayaram, and T. Fiez, "Efficient far field energy harvesting for passively powered sensor networks," *IEEE J. Solid-State Circuits*, Vol. 43, No. 5, 1287–1302, 2008.
6. Scorcioni, S., L. Larcher, and A. Bertacchini, "A reconfigurable differential CMOS RF energy scavenger with 60% peak efficiency and 21 dBm sensitivity," *IEEE Microw. Wireless Compon. Lett.*, Vol. 23, No. 3, 155–157, 2013.

7. Liu, N. W., L. Zhu, W. W. Choi, and J. D. Zhang, "A differential fed microstrip patch antenna with bandwidth enhancement under operation of TM_{10} and TM_{30} modes," *IEEE Trans. Antennas Propag.*, Vol. 65, No. 4, 1607–1614, 2007.
8. Arrawatia, M., M. S. Bhaghni, and G. Kumar, "Differential microstrip antenna for energy harvesting," *IEEE Trans. Antennas Propag.*, Vol. 63, No. 4, 1581–1588, 2015.
9. See, T. S. P., X. Qing, W. Liu, and Z. N. Chen, "A wideband ultra-thin differential loop fed patch antenna for head implants," *IEEE Trans. Antennas Propag.*, Vol. 63, No. 7, 3244–3248, 2015.
10. Han, L., W. Zhang, X. Chen, G. Han, and R. Ma, "Design of a compact differential dual frequency antenna with stacked patches," *IEEE Trans. Antennas Propag.*, Vol. 58, No. 4, 1387–1392, 2010.
11. Hu, H. T., F. C. Chen, J. F. Qian, and Q. X. Chu, "A differential filtering microstrip antenna array with intrinsic common mode rejection," *IEEE Trans. Antennas Propag.*, Vol. 65, No. 12, 7361–7365, 2017.
12. Pepe, D., L. Vallozi, H. Rogier, and D. Zito, "Planar differential antenna for short range UWB pulse radar sensor," *IEEE Antennas Wirel. Propag. Lett.*, Vol. 12, 1527–1530, 2013.
13. Wu, H., J. Zhang, L. Han, R. Yang, and W. Zhang, "Differential dual-band antenna-in-package with T-shaped slots," *IEEE Antennas Wirel. Propag. Lett.*, Vol. 11, 1446–1449, 2012.
14. Jin, H., W. Che, K. S. Chin, G. Shen, W. Yang, and Q. Xue, "60 GHz LTCC differential fed patch antenna array with high gain by using soft surface structures," *IEEE Trans. Antennas Propag.*, Vol. 65, No. 1, 206–216, 2017.
15. Wang, Y., F. Zhu, and S. Gao, "Design and investigation of a differential fed UWB patch antenna with polarization diversity," *International J. of Antennas and Prop.*, ID. 4254830, 2016.
16. Tang, Z., J. Liu, and Y. Yin, "Design and measurement of a differential printed antenna for a wireless sensor node," *IEEE Antennas Wirel. Propag. Lett.*, Vol. 16, 2228–2231, 2017.
17. Gadhafi, R., D. Cracan, A. Mustapha, and M. Sanduleanu, "An H-shaped differential antenna for 5G/FR1 applications," *IEEE MTT-S Latin America Microwave Conference*, Arequipa, Peru, December 12–14, 2018.
18. Zito, D. and D. Pepe, "Planar differential antenna design and integration with pulse radar microchip sensor," *IEEE Sensor J.*, Vol. 14, No. 8, 2477–2487, 2014.
19. Kumar, G. and K. P. Ray, *Broadband Microstrip Antennas*, Artech House, 2002, ISBN 1-58053-24-6.
20. Meys, R. and F. Janssens, "Measuring the impedance of balanced antennas by an S -parameter method," *IEEE Antennas Propag. Mag.*, Vol. 40, No. 6, 62–65, 1998.
21. Zhang, Y. P. and J. J. Wang, "Theory and analysis of differentially-driven microstrip antennas," *IEEE Trans. Antennas Propag.*, Vol. 54, No. 4, 1092–1099, 2006.
22. Chouchene, W., C. Larbi, and T. Aguilu, "New electrical equivalent circuit model of the inset fed rectangular patch antenna," *2017 Progress In Electromagnetics Research Symposium — Spring (PIERS)*, 646–651, St Petersburg, Russia, May 22–25, 2017.
23. Electrical Specifications Data Sheet [Online], available at www.markimicrowave.com/Assets/data-sheets/BAL-0106.pdf.
24. Gadhafi, R. and M. Sanduleanu, "A modified patch antenna with square-open loop resonator slot for improved bandwidth performance for in WiFi applications," *Adv. in Science, Tech. and Engineering Systems J.*, Vol. 2, No. 3, 1467–1471, 2017.